

Optimized ^{31}P MRS in the human brain at 7T with a dedicated RF coil setup

Bart L. van de Bank^a, Stephan Orzada^b, Frits Smits^a, Miriam W. Lagemaat^a, Christopher T. Rodgers^c, Andreas K. Bitz^{b,d} and Tom W. J. Scheenen^{a,b,*}

The design and construction of a dedicated RF coil setup for human brain imaging (^1H) and spectroscopy (^{31}P) at ultra-high magnetic field strength (7 T) is presented. The setup is optimized for signal handling at the resonance frequencies for ^1H (297.2 MHz) and ^{31}P (120.3 MHz). It consists of an eight-channel ^1H transmit–receive head coil with multi-transmit capabilities, and an insertable, actively detunable ^{31}P birdcage (transmit–receive and transmit only), which can be combined with a seven-channel receive-only ^{31}P array. The setup enables anatomical imaging and ^{31}P studies without removal of the coil or the patient. By separating transmit and receive channels and by optimized addition of array signals with whitened singular value decomposition we can obtain a sevenfold increase in SNR of ^{31}P signals in the occipital lobe of the human brain compared with the birdcage alone. These signals can be further enhanced by $30 \pm 9\%$ using the nuclear Overhauser effect by B_1 -shimmed low-power irradiation of water protons. Together, these features enable acquisition of ^{31}P MRSI at high spatial resolutions (3.0 cm^3 voxel) in the occipital lobe of the human brain in clinically acceptable scan times (~ 15 min). © 2015 The Authors. *NMR in Biomedicine* published by John Wiley & Sons Ltd.

Keywords: ^{31}P -MRS; ^{31}P -MRSI; spectroscopic imaging; ultra-high field; RF coil; array coil; multi-transmit; B_1 shimming; WSVD; 7 T

INTRODUCTION

For many years now, examining the local distribution of metabolites containing phosphorus (^{31}P) atoms in the human brain has been done non-invasively by *in vivo* ^{31}P -MRSI (1). This can give insight in determining or understanding specific metabolic processes, such as energy metabolism or cell membrane turnover. Metabolites of interest for these processes are phosphocreatine (PCr), adenosine triphosphate (ATP), inorganic phosphate (P_i) and the phosphomono- and diesters, which can be directly observed *in vivo* by ^{31}P spectroscopy.

The sensitivity of the ^{31}P nucleus is lower than that of the ^1H nucleus ($\gamma^1\text{H}/\gamma^{31}\text{P} = 2.4$), but both improve with increasing B_0 . Moreover, ^1H B_1 homogeneity becomes a real challenge in larger volumes at higher field strengths (≥ 7 T), but this is less so for ^{31}P . Rodgers *et al* found a 2.8-fold increase for ^{31}P -MRS in the human heart when going from 3 T to 7 T (2). The complexity of spectral patterns of ^{31}P -MRS is reduced compared with ^1H spectra, because fewer metabolites have a ^{31}P nucleus present, and fewer resonances overlap.

Dedicated hardware is needed to detect MR signals from ^{31}P nuclei. A clever design of this hardware can contribute to an improved signal-to-noise ratio (SNR) for detection of these signals. RF surface coils, regardless of their operating frequency, have been frequently used for their excellent, albeit spatially constrained, SNR (3). A drawback of RF surface coils is their inhomogeneous B_1 field, requiring complex high-power adiabatic pulses to homogeneously excite a region of interest (ROI) close to the coil (4). Instead, a fairly uniform flip can be achieved by using volume coils, of course depending on the size of the sample and the operating frequency of the coil. This enables the use of short hard pulses instead of longer adiabatic pulses, as has been shown by Avdievich and

Hetherington at 4 T (5). When separating the excitation and reception of MR signals by designing a volume RF coil for excitation and

* Correspondence to: T.W.J. Scheenen, Department of Radiology and Nuclear Medicine, Geert Grooteplein-zuid 10, huispost 766, P.O. Box, 9101, 6500 HB, Nijmegen.
E-mail: tom.scheenen@radboudumc.nl

a. B. L. van de Bank, F. Smits, M. W. Lagemaat, T. W. J. Scheenen
Department of Radiology and Nuclear Medicine, Radboud University Medical Center, Nijmegen, The Netherlands

b. S. Orzada, A. K. Bitz, T. W. J. Scheenen
Erwin L. Hahn Institute, University Hospital Duisburg-Essen, Essen, Germany

c. C. T. Rodgers
Oxford Centre for Clinical Magnetic Resonance Research (OCMR), University of Oxford, John Radcliffe Hospital, Oxford, UK

d. A. K. Bitz
Medical Physics in Radiology, German Cancer Research Center (DKFZ), Heidelberg, Germany

This is an open access article under the terms of the Creative Commons Attribution License, which permits use, distribution and reproduction in any medium, provided the original work is properly cited.

Abbreviations used: $|E|$, absolute component of electric field; $|H|$, absolute component of magnetic field; ^1H , proton; ^{31}P , phosphorus-31; ATP, adenosine triphosphate; BC, birdcage; CH, channel; CP mode, circularly polarized mode (quadrature driven); FOV, field of view; GPC, glycerophosphocholine; GPE, glycerophosphoethanolamine; NOE, nuclear Overhauser effect; PC, phosphocholine; PCr, phosphocreatine; PE, phosphoethanolamine; P_i , inorganic phosphate; Q_L , quality factor in loaded condition; Q_U , quality factor in unloaded condition; ROI, region of interest; Rx, signal reception; S_{12} , transmission coefficient; SAR, specific absorption rate; SNR, signal-to-noise ratio; T_{acq} , total acquisition time; TEM, transverse electromagnetic; Tx, signal transmission; VNA, vector network analyzer; WSVD, whitened singular value decomposition.

a receive array for acquisition, adiabatic pulse shapes can be avoided and excellent SNR can still be achieved by receiving with small elements (2,3,6,7). The signals from each of these elements must then be combined optimally, which can be achieved with the whitened singular value decomposition (WSVD) method (8,9).

The ^{31}P RF coil setup needs to be integrated into another RF coil that handles ^1H signals. In contrast to clinical MR systems (at $B_0 \leq 3\text{ T}$), no whole body RF coil is provided as standard within human 7 T systems (10). Therefore, local ^1H RF coils must be employed to excite the proton spins and receive their signals, to obtain anatomical images and to be able to optimize the field (B_0 and B_1 shimming). The short wavelengths produce inhomogeneous RF fields; these destructive interferences can coincide within an ROI, decreasing signal intensity at the desired location. When using multiple signal transmission (Tx) coil elements, it is possible to adjust the transmitted RF field by changing input phases and amplitudes of the RF pulses to remove (or shift) these interferences outside the ROI, known as B_1 shimming (11). When multiple coil elements are integrated within a multi-transmit proton coil it must be assured that local specific absorption rate (SAR) hot-spots are minimized and remain within guidelines. If by B_1 shimming proton signals of water can be irradiated with low RF power, the nuclear Overhauser effect (NOE) (12) can be used to increase the steady state magnetization of certain ^{31}P nuclei surrounded by water, potentially providing an additional sensitivity to a ^{31}P experiment. This enhancement technique can be used in any organ as long as sufficient power to excite the ^1H spins can be delivered to the ROI. Positive NOE enhancements have been reported for prostate and brain ^{31}P MRSI at 7 T (13,14). Other techniques, such as INEPT, can also be used to enhance signals of the ^{31}P compounds, as has been shown for 3 T (15,16) and even for 7 T (17,18). However, as these techniques use rather complex sequences with several inversion pulses, reaching the correct flip angle and not running into SAR restrictions is a major issue. Moreover, T_2 relaxation during long spin evolution times at 7 T could decrease or even negate the polarization gain.

Our aim was to design and construct an integrated coil setup optimized for efficient NOE, uniform ^{31}P spin excitation and high SNR ^{31}P MRS(I) for 7 T. This safety-validated coil setup should allow optimization of the ^1H transmit field (B_1 shimming) and standard ^1H imaging as well as uniform excitation and acquisition of ^{31}P spins throughout the human brain, with a possibility of using an additional local receive array and without removing the coil or the patient during an examination. Therefore, we combined an eight-channel (8-CH) multi-transmit head coil (^1H) with a newly constructed and insertable actively detunable volume resonator (^{31}P), and developed a 7-CH receive-only (Rx) array (^{31}P) that improves SNR locally. Together with optimized signal addition and the possibility to use B_1 -shimmed NOE the sensitivity of local ^{31}P signal detection is maximized.

MATERIALS AND METHODS

RF coil design and construction

The complete coil setup consists of three parts: an 8-CH ^1H transmitter array (TxRx), an actively detunable ^{31}P volume resonator and a ^{31}P 7-CH Rx array. Note that the ^{31}P volume resonator can be used as transmitter (without Rx array) and as transmit only (with Rx array).

^1H TxRx array

As basis for the complete setup we chose to use an existing ^1H head coil designed by Orzada *et al.* (19). This coil has an octagonal shaped construction and consists of eight intrinsically decoupled microstrip elements with meanders that can be used in multi-transmit mode (20). Each element was tuned to the resonance frequency of 297.2 MHz and matched to $50\ \Omega$ when loaded and with the birdcage (BC) inserted. Cable traps tuned to the resonance frequency of ^{31}P were added to all individual elements.

^{31}P volume resonator (TxRx)

The ^{31}P coil was designed as a BC coil to allow uniform excitation of the ^{31}P signals in the human brain, which should fit inside the 8-CH head coil. Therefore, we created an eight-rung, high-pass design. This design avoids interference of the resonant modes with the 8-CH head coil, as the highest useful resonance is the dominant mode (21). This eight-rung design also ensures that the rungs could be positioned exactly between the eight ^1H microstrip elements (Fig. 1B).

The BC was created with copper foil (Parker Chomerics CHO-FOIL[®], Parker Hannifin Corporation, Woburn, MA, USA) attached to a Plexiglas tube (\varnothing_{out} 24 cm, length 25 cm, thickness 0.5 cm). We enlarged the diameter to 25 cm by opening the tube at one side over the complete length. The opening was fixed by two small Plexiglass parts ($1 \times w\ 3.2 \times 3.2\text{ cm}^2$), which supported the end rings. Two rings of copper foil (width 12.5 mm) were attached to the tube with a spacing of 155 mm. Between the end rings, a total of eight rungs (length 15.5 cm, width 4.5 mm) were placed equidistantly around the tube. A smaller width of the rungs compared with the end rings was chosen to minimize distortion of the ^1H field (Fig. 2). The BC was tuned to 120.3 MHz (loaded), by soldering a total capacitance of 14.7 pF in the end rings between the rungs, where a capacitance of 16 pF had been determined with BirdcageBuilder (22). Two tank circuits were added to each rung. Symmetry was preserved by positioning them at both ends. These circuits cause a high impedance at the frequency of 297.2 MHz, while a low impedance is present at 120.3 MHz, hence minimizing the coupling to the ^1H elements and optimizing tuning to the ^{31}P Larmor frequency (23). Additionally, a PIN-diode was placed in series (Fig. 1A) to actively detune the BC during signal acquisition and to enable the use of a local receive array coil. The BC coil had two ports and was driven in circularly polarized (CP) mode (quadrature mode, fixed phase difference of 90° between the two ports). Each port was matched to the characteristic impedance of the MR system ($50\ \Omega$) by increasing the matching capacitors to 15.6 pF and by decreasing the capacitors in the opposing end ring to 13.9 pF. The ports were isolated by replacing the capacitors between the matching circuits and the other end ring by 27 pF and by reducing the values of both capacitors that were in the same plane to 8.6 pF. Cable traps tuned to 120.3 MHz to balance the input and to filter common-mode currents were inserted between the matching circuit and the connection to the MR system.

Array coil (Rx only)

A 7-CH Rx array coil was developed to further improve the SNR of signals arising from ^{31}P compounds. Each circular loop (channel) was made from copper wire (wire diameter 1.25 mm^2), having a loop radius of approximately 25 mm and having four symmetrically distributed fixed tuning capacitors (68 pF each). Each loop was matched to $50\ \Omega$ (loaded) by placing an additional

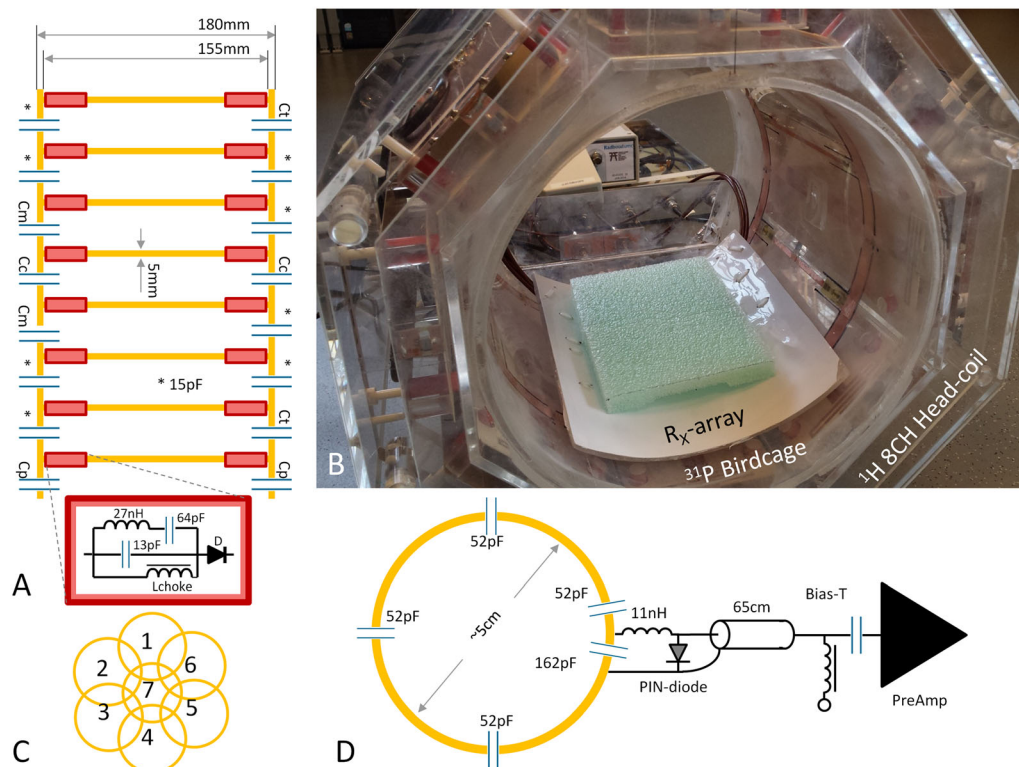


Figure 1. Overview of the complete setup, with detailed representations of the newly designed, detunable ^{31}P BC insert and ^{31}P Rx array. (A) Schematic representation of the eight-rung high-pass BC coil; included are details of the tank and detune circuits (red box). Capacitor values used to tune and match the BC coil were $C_m = 15.6\text{ pF}$, $C_t = 13.3\text{ pF}$, $C_c = 27\text{ pF}$ and $C_p = 10\text{ pF}$. (B) The octagonal-shaped 8-CH ^1H head coil was used as the basis for the insertable, detunable ^{31}P BC coil, which could host the additional 7-CH Rx array coil. (C) Schematic configuration of the 7-CH Rx array. (D) A pictorial overview of a single element of the 7-CH Rx array, where each adjacent element is decoupled by overlap and by pre-amplifier decoupling.

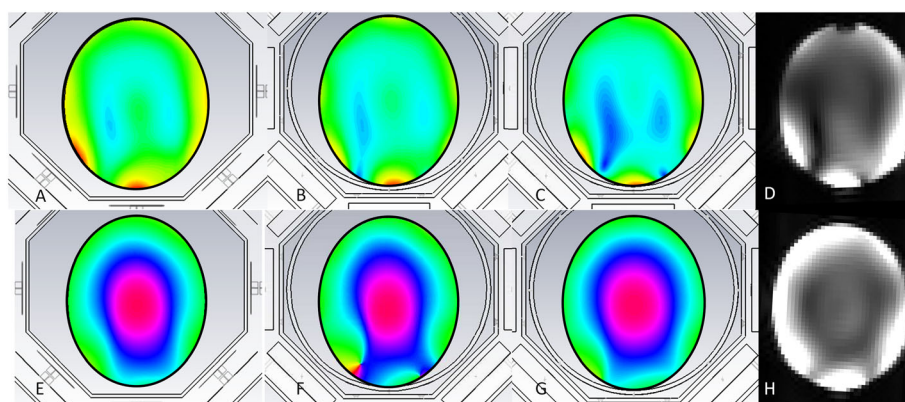


Figure 2. (A–C, E–G) Simulation of proton magnetic field (A–C) and phase (E–G) distribution of the 8-CH head coil, with and without the ^{31}P BC inserted into the 8-CH setup. (A, E) The field and phase distributions of the 8-CH head only, (B, F) the distribution when the BC is inserted (in this case the legs had a width of 12.5 mm), (C, G) the distribution when the width of the legs is reduced to 4.5 mm. (D, H) ^1H images of the same phantom with the BC present in the setup; the image in D corresponds to the simulation result as presented in C, hence showing equal field distribution. In H the field distribution is shown with the tank circuits inserted into the BC.

capacitor (162 pF), which was also part of the active detuning network, in the loop. Part of this active detuning is the parallel positioned PIN-diode. To create a high impedance at the resonance frequency in the loop, a small inductor of 11 nH was added between the PIN-diode and the matching capacitor (Fig. 1D). Mutual inductance was minimized by overlapping adjacent loops. Coupling between non-overlapping loops was reduced by pre-amplifier decoupling, which transformed the low impedance of the pre-amplifier to a high impedance at the coil (6,7).

MR hardware and RF interfaces

All experiments were performed on a 7 T whole body MR system (MAGNETOM 7 T, Siemens Healthcare, Erlangen, Germany). The 8-CH ^1H coil was driven by eight 1 kW RF amplifiers (LPPA 13080 W, Dressler, Germany), where the amplitude and phase of each channel could be altered using a vector modulator, enabling B_1 shimming (11). The TxRx switches with pre-amps were placed in a separate box at the head of the patient table.

A single 8 kW RF amplifier was used to excite the ^{31}P signal (LPPA 13080 W-CAN, Dressler, Germany). This signal was divided and phased by a lumped-element quad-hybrid to drive the BC in quadrature mode. The ^{31}P receive array was connected to a homebuilt 7-CH receive interface box optimized for signal acquisition at 120.3 MHz, where in each receive-path an improved tank circuit (23) was added to trap proton signals. For safety we added to the interface a PIN-diode breakdown detection circuit, that immediately stops the scanner if a PIN-diode malfunctions or when a cable is disconnected.

Functionality and safety tests

Bench tests

The BC was tested in TxRx mode and in Tx mode. In the latter case, the coil must be detuned while receiving the MR signal with the local Rx setup. Active tuning was verified by measuring the transmission coefficient (S_{12}) of the BC, by using two loosely coupled pick-up probes that were connected to a vector network analyzer (VNA) (R&HZVL3, Rohde & Schwarz, Munich, Germany). This setup was also used to determine the ratio of unloaded-to-loaded quality factors (Q_U/Q_L) (24).

For the receive array, we assessed active detuning, determined the crosstalk between each element, and determined the ratio of unloaded-to-loaded quality factors (Q_U/Q_L) for each element. Active detuning was checked by switching the currents to the PIN-diode between forward and reverse bias, while measuring the effect of the S_{12} response of two pick-up loops that were weakly coupled to the element under investigation. This method was also used to determine the Q -factor. Crosstalk between elements was determined by connecting the elements under investigation to the network analyzer, probing signal through one of the elements and receiving with the other. Note that only the element under investigation was tuned and all other coil elements were detuned while making these measurements.

Simulations and RF field measurements

Simulations (CST Studio Suite, CST AG, Darmstadt, Germany) of the setup were made to assess homogeneity of the ^1H -field and to investigate couplings between the two volume coils. Those simulations were performed with and without the BC inserted in the 8-CH head coil. The receive array was not used in the simulations, but validated with bench measurements. We assumed that existing SAR simulations for the 8-CH head coil could be maintained when field homogeneity was not altered by the insert (19,25). We validated these simulations, and the possible additional influence of the ^{31}P Rx array, by assessing the $|H|$ - and $|E|$ -field distributions at both resonances in a phantom filled with head tissue simulating liquid (^{31}P , $\epsilon_r = 76.5$, $\sigma = 0.78 \text{ S/m}$; ^1H , $\epsilon_r = 56.3$, $\sigma = 0.98 \text{ S/m}$). Field probes (Schmid & Partner Engineering AG (SPEAG), Zürich, Switzerland, probes H3DV7 & ES3DV2) were used to collect the maps in a sagittal ($\text{AP} \times \text{FH}$ $190 \times 190 \text{ mm}^2$) and coronal ($\text{LR} \times \text{FH}$ $160 \times 190 \text{ mm}^2$) plane in the phantom. Data were collected every 10 mm while probing through the complete coil setup with and without the ^{31}P Rx array insert at the desired frequency (1 W). Both planes were positioned along the midline of the phantom (Fig. 3A).

^{31}P MR of phantom and volunteers

The complete functionality of the coil setup was checked with the following tests: (i) 90° flip angle calibration of the BC, (ii) determination of the SNR increase of the ^{31}P signal when acquiring data with the Rx array instead of the BC, (iii) obtaining the noise correlation matrix of the 7-CH Rx array, and (iv) ^1H B_1^+ shimming with all ^{31}P components present. For these tests a cylindrical phantom (diameter 16 cm and volume $\sim 5 \text{ L}$) filled with inorganic phosphate (P_i) (30 mM) (and 2% agar) was used. For an additional *in vivo* test two healthy volunteers (males, 24 years and 26 years) were scanned after giving written informed consent.

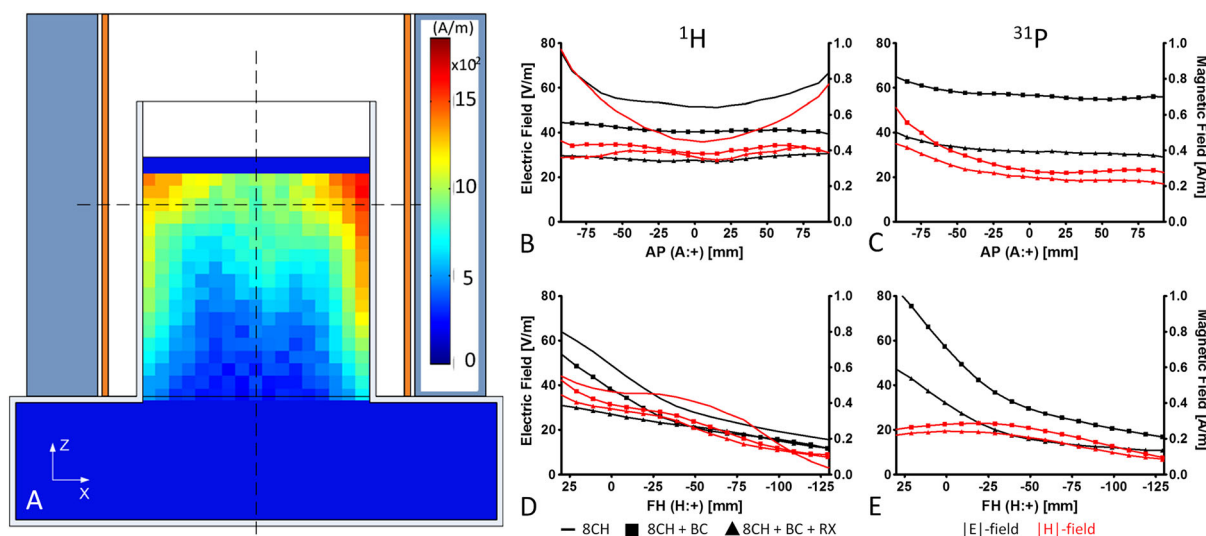


Figure 3. Results of the validation measurements using the field probes. (A) Two-dimensional visualization of the coil setup surrounding the head-shoulder phantom as it was used to determine the magnitude of the $|E|$ and $|H|$ fields with the field probes. Included is a map of the proton $|H|$ field as it was measured with the 8-CH head coil only. The phantom was filled with tissue-simulating fluid, having a conductivity of 0.98 S/m for ^1H and 0.78 S/m for ^{31}P , and a permittivity of 56.3 for ^1H and 76.5 for ^{31}P . (B–E) Profiles for each individual $|E|$ - and $|H|$ -field measurement (these profiles were taken along the dashed lines (A)) with (B, D) ^1H and (C, E) ^{31}P . These measurements were made (i) for the 8-CH head coil only, (ii) for the 8-CH head coil with ^{31}P BC inserted and (iii) for the complete setup with receive coil. These measurements were corrected for input power and hence are directly comparable to those of Reference 25. Note that $|E|$ and $|H|$ fields decrease when more components are present.

A repeated slice selective pulse acquire sequence (6 ms excitation pulse (sinc), $T_R = 15$ s, single shot) selecting a 40 mm thick axial slice through the center of the coil was used for flip angle calibration, where the RF amplitude of the excitation pulse was varied to find the maximum amplitude of the peak present in the phantom (P_i), which approximates a 90° excitation.

Two 3D MRSI data sets of the same cylindrical phantom were obtained to determine the SNR performance of the ^{31}P coils. In both experiments, we excited the ^{31}P signal using the BC, but acquired the signal with the BC in one, and acquired the signals with the ^{31}P Rx array in the other experiment. Signals from the individual receive channels were combined using the WSVD combination method (8), comprising (i) a very short noise prescan that is used to decorrelate the single-element spectra (or FIDs) and (ii) computation of the maximum likelihood combined spectrum. The Rx array was not present in the first test with the BC alone, thus before the second test the phantom was accurately repositioned after the Rx array was inserted. The 3D pulse-acquire MRSI experiment had the following parameters: T_R /acquisition delay 1000/0.1 ms, flip angle 40° , hard pulse duration 0.3 ms, field of view (FOV) $240 \times 240 \times 200 \text{ mm}^3$, matrix $12 \times 12 \times 8$, elliptical k -space acquisition with 100% Hamming filter, vector size 1024 and T_{acq} 5 min 15 s. The spectra from the MRSI data were fitted with Metabolite Report, a work in progress package from Siemens Healthcare (Erlangen, Germany). Metabolite Report performs automated, prior-knowledge-based, complex fitting in the time domain and has previously been applied to 7 T ^{31}P spectroscopy data of the prostate (13). Images of the fitted P_i signal were created by interpolating its initial $12 \times 12 \times 8$ matrix to a $256 \times 256 \times 8$ matrix. They were then convoluted by a disk-shaped kernel and masked. These images were then used to determine the local signal gain when using the Rx array as compared with the BC. An additional examination without RF excitation pulses was performed to obtain the noise correlation matrix.

In an *in vivo* study we investigated the ability to use B_1 shimming and the ability to acquire 3D ^{31}P MRSI in the human brain with and without NOE enhancement on a single volunteer (24 years) (T_R /acquisition delay 1500/0.10 ms, flip angle 45° , matrix $12 \times 12 \times 8$, FOV $240 \times 240 \times 240 \text{ mm}^3$, pulse length 0.3 ms, elliptical k -space acquisition with 100% Hamming filter, $T_{\text{acq}} = 7$ min 48 s). A high-resolution 3D ^{31}P MRSI using NOE enhancement with an approximated true voxel size of 3.0 cm^3 was acquired from the second volunteer (26 years). This time data was collected with the Rx array, providing a reduced FOV. Parameters used for this sequence were T_R /acquisition delay 500/0.10 ms, flip angle 30° , FOV $140 \times 140 \times 100 \text{ mm}^3$, matrix $14 \times 14 \times 10$, NSA = 6 and T_{acq} 15 min 2 s; all other parameters were kept the same. As the T_R is reduced and we want the maximum signal per unit time, we reduced the flip angle to the Ernst angle for PCr (30°) with $T_1 = 3.4 \pm 0.3$ s (14). In each examination the NOE enhancement was generated by saturating the water signals ($\gamma B_1 = 30$ Hz) using the wideband alternating-phase low-power technique for zero residual splitting (WALTZ-4, technique originally intended for decoupling) (26) during the full T_R except during the 204 ms of signal acquisition. Other examinations within the protocol were the same for both volunteers. After B_0 and B_1 shimming the whole brain, a 3D T_1 -weighted image was acquired with an MPRAGE (magnetization prepared rapid acquisition gradient echo) pulse sequence. For this sequence the following parameters were used: $T_R/T_1/T_E$ 2500/1100/1.270 ms, resolution 1 mm^3 , T_{acq} 3 min 58 s. Then we calibrated the flip angle for ^{31}P , and we optimized the B_1 shim for the occipital lobe.

RESULTS

Bench tests

RF coils

The ratio of unloaded-to-loaded quality factors (Q_U/Q_L) for the BC was $110/30 = 3.7$. For the receive array it was $(155 \pm 20)/(63 \pm 5) = 2.7 \pm 0.3$, with a range of 124–181 for Q_U and 57–69 for Q_L .

Simulations and RF field measurements

Simulations were used to determine the influence of the ^{31}P BC at the ^1H field when it is inserted into the 8-CH head coil. These showed that standard 12.5 mm wide copper tape for the legs created a signal void a few centimeters inside the phantom: coinciding with this void was a phase singularity (Fig. 2B, F). Simulations showed that the signal void and the phase singularity could be removed when the width of the legs was reduced to 4.5 mm (Fig. 2C, G), although with reduced sensitivity. The sensitivity increased and could be related to the field intensity of the 8-CH head-coil without BC when the tank circuitry was added to the BC (Fig. 2H).

The field probe measurements visualized the field distribution for both nuclei. For the ^1H field in general, we concluded that the overall field distribution in the phantom was comparable to that from the reference coil (25), but that amplitudes in the center had been decreased for this new setup. This was shown by the coronal map of the $|H|$ field at 297 MHz for the 8-CH head coil only (Fig. 3A). Note that the 8-CH head coil was tuned and matched to the resonance frequency with the BC inserted.

The proton $|H|$ - and $|E|$ -field amplitudes at both resonances for the coil assembly in different configurations (Fig. 3) illustrated that the amplitudes of both field types decreased with the BC inserted. Signals did not decrease further with the Rx coil present. Moreover, the stronger decrease in $|E|$ field (causing SAR deposition) compared with the $|H|$ field confirmed that it was safe to use this coil assembly with the original 8-CH safety margins.

Comparing these results with the 8-CH proton setup without any additional coils (19,25) enabled us to use the same maximal permissible input power, since the magnitude of the electric field is reduced after insertion of the additional components, providing an even greater safety margin in the case of the new ^1H coil assembly. For ^{31}P the maximum permissible input power was calculated based on a worst-case approximation (losses in the feeding network and RF coil were neglected) for the head-averaged SAR according to the rationale given in the IEC 60601-2-33 for volume transmit coils: $P_{\text{max}}^{31\text{P}} = \text{SAR}_{\text{head,limit}} m_{\text{head}}$.

^{31}P MR of phantom

Calibration of the RF power to reach a 90° flip angle for the ^{31}P signals in a phantom as well as in the human brain showed that the maximum signal intensity coincided with a reference B_1^+ amplitude of $29 \mu\text{T}$. This resulted in a maximum achievable B_1^+ amplitude for ^{31}P of approximately $56 \mu\text{T}$ for this coil setup (on average this value was a little lower, 45–50 μT).

The noise correlation matrix (Fig. 4) confirmed that coupling between all elements was minimized as a result of overlap and pre-amplifier decoupling. The average noise correlation over all elements was $10 \pm 7\%$, with its maximum of 23% found between elements 3 & 6.

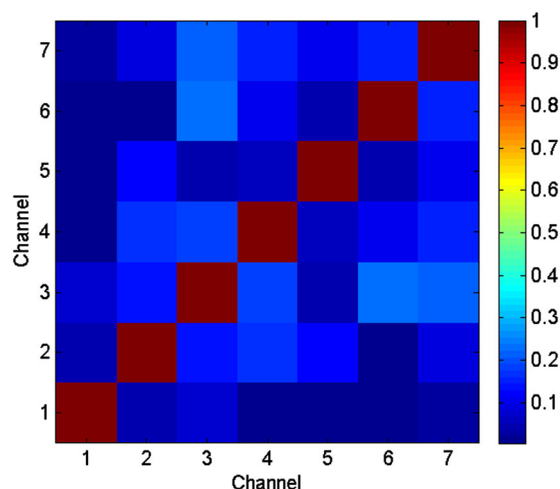


Figure 4. Noise correlation matrix of the 7-CH Rx array. All channels are properly decoupled, because noise does not correlate significantly. The average noise correlation over all elements was $10 \pm 7\%$, with its maximum of 23% found between elements 3 and 6.

As expected, the SNR increased substantially when the Rx array was used for signal acquisition as compared with the BC. An increase in SNR was visible up to 7 cm inside the phantom, with a sevenfold increase up to 2 cm inside the phantom (Fig. 5).

^{31}P MR of volunteers

The *in vivo* experiments were successful. We could obtain detailed T_1 -weighted images with the 8-CH ^1H head coil driven in CP+ mode (Fig. 6, background) and were able to shim the ^1H B_1^+ field (Fig. 6A–C). This allowed us to maximally enhance ^{31}P signals using a B_1 -shimmed setting for specified regions. For the whole brain, we plotted the metabolite map of PCr when measured with and also without NOE enhancement (Fig. 6D, E). An enhancement map showed the signal increase, expressed as a percentage (Fig. 6F); the main features of this enhancement map coincided with the ^1H B_1^+ field (Fig. 6C). The overall enhancement of the PCr signal was $30 \pm 9\%$.

When acquiring signals with the local receive array, we could reduce the FOV and hence increase spatial resolution. Combined with local NOE enhancement and an optimized signal combina-

tion method (i.e. WSDV combination), we obtained ^{31}P spectra from relatively small voxels (3.0 cm^3) in 15 min, with narrow linewidths for PCr ($9.6 \pm 1.9\text{ Hz}$) and high SNR (17.8 ± 3.7) (Fig. 7), up to 5 cm into the occipital lobe.

The SAR for the experiments with NOE enhancement was evaluated using the real-time SAR monitoring system (27). The time-averaged total input power for these experiments (not incorporating coil losses) was 10.9 W for ^1H and 2.2 W for ^{31}P .

DISCUSSION

In this work, we have described the design, construction, and safety validation of a dedicated coil setup for 7 T containing three main components: an 8-CH multi-transmit ^1H head coil, an insertable and actively tunable BC coil for ^{31}P and a local 7-CH ^{31}P Rx array. The setup featured multi-transmit capabilities on the ^1H channels, volume excitation for ^{31}P , and a large local SNR improvement close to the receive array. This increase in sensitivity in combination with the limited FOV of local receive coils enabled ^{31}P MRSI at higher spatial resolution, and may be used to reduce scan time.

The tuning and matching of the 8-CH ^1H head coil had to be adapted, because its initial tuning frequency dropped below the resonance frequency of the system. Therefore we tuned it to the correct frequency and adapted the matching to become 50 Ω (loaded) with the BC present. Despite this adaption, we noticed a reduction in sensitivity of the ^1H signal, which is probably caused by the large quantity of conductive material present in the BC itself. Although this might block part of the signal, as reported for high-density receive arrays (28), we did not observe a change in the shape of the field distributions in the phantom measurements.

Although not shown here, it is worth noting that the homogeneity of the BC was hardly altered by the addition of the local Rx array. Each element in the receive array was actively detuned, meaning that a current was used to forward bias a parallel positioned PIN-diode, bringing the element off resonance during BC transmit. We added no additional safety features, such as a second trap with passive diodes (29) or an RF fuse, to the individual loops in order to avoid a possible decrease in SNR. Instead, we considered (and verified) that, should a parallel-positioned

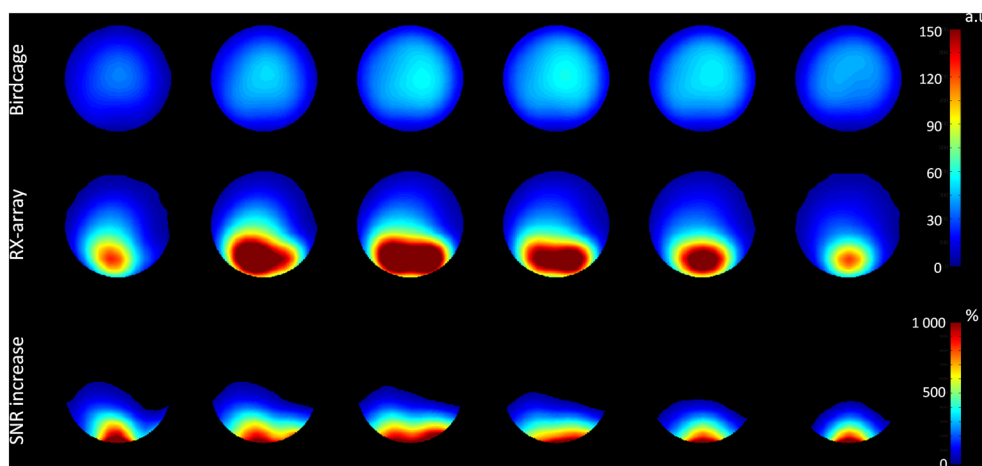


Figure 5. Interpolated SNR images of a spherical phantom containing 30 mM inorganic phosphate. The images were obtained with the BC coil (top row) and with the local Rx array (middle row). The gain in SNR is more than sevenfold close to the receive array. Also note the uniform B_1 field when data was solely acquired with the BC.

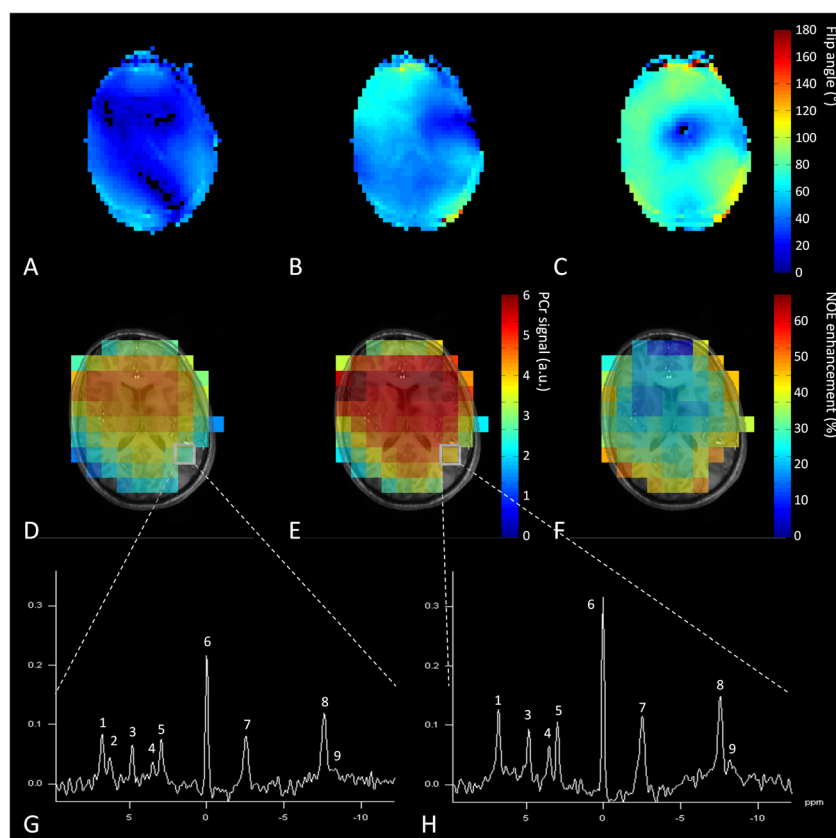


Figure 6. (A–C) Results of *in vivo* experiment using the complete setup showing different B_1^+ maps of the ^1H field: (A) in CP- mode, (B) homogenized for the complete brain, and (C) locally optimized for occipital lobe. Showing the ability to use B_1 shimming with the coil setup. Background images were acquired with the 8-CH ^1H head coil driven with global B_1 optimization, showing fairly homogeneous field distribution. (D–F) ^{31}P spins were excited and signal was acquired with the BC (D) without and (E) with NOE enhancement of PCr; (F) the global enhancement map. (G, H) An example of ^{31}P spectra taken from the same voxel (G) without NOE enhancement and (H) with NOE enhancement. Spectra were obtained in 7 min 48 s with an approximate voxel size of 38 cm^3 . The metabolites present in these spectra are (1) phosphoethanolamine (PE), (2) phosphocholine (PC), (3) P_i , (4) glycerophosphoethanolamine (GPE), (5) glycerophosphocholine (GPC), (6) PCr, (7) γ -ATP, (8) α -ATP and (9) NADH.

PIN-diode break down, a short circuit would be created and hence the coil element would be detuned, which makes it intrinsically safe. However, this feature does not detect a moment when no current flows through the PIN-diode (e.g. when a cable is disconnected). Therefore, we added a current sensing circuit inside the interface, which activates and stops the scanner immediately if no current goes to the PIN-diods.

The SNR increase by exciting the spins via the BC and receiving their signal with the array coil may have been biased, as the BC for reception may have had degraded performance. The PIN-diods for tuning the BC were positioned in series within the legs: when forward biased (tuned) they have a low additional series resistance; when the PIN-diods are reverse biased (detuned) this resistance will increase significantly. However, the coil has a relatively high Q_U (110), and when the Q_U/Q_L ratio is above 3.5 tissue loading dominates over coil losses. Hence, the introduction of PIN-diods in the BC did not degrade its performance in the first place.

Increasing SNR by separating Rx and Tx surface coils for ^{31}P spectroscopy has been reported before (30,31), where Avdievich and Hetherington were the first to design and develop a homogeneous transmit volume coil (5), which was the basis for our work. Their coil was designed as an actively detunable double-tuned transverse electromagnetic (TEM) head coil for 4 T. The two setups have similar properties and both can provide

anatomical reference images and ^{31}P MRSI of the patient without removal of the coil or the patient. The advantage of our design over theirs is the ability to use B_1 shimming. Moreover, the size of the individual elements of the Rx ^{31}P array in our design was smaller, resulting in a local increase in SNR.

It was shown by Lei *et al.* that signal from PCr in the human brain can be increased by $24.3 \pm 1.6\%$ using NOE (14). However, this effect depends on the amplitude and distribution of the ^1H B_1 field (Fig. 6C, F) and can therefore vary spatially (13). This principle can be exploited to enhance specific regions. If NOE is used, it is essential to reach a threshold ^1H B_1^+ value in a certain area to achieve maximum NOE enhancement. An additional ^1H B_1^+ map is therefore needed to assess the locations where the threshold B_1^+ was reached. ^{31}P B_1^+ does not affect the NOE variation. With the current coil setup, an overall enhancement of $30 \pm 9\%$ for the PCr signal could be reached in the human brain. This higher enhancement compared with the data of Lei *et al.* may be related to the proton irradiation power of this coil and our choice of the WALTZ-4 decoupling strategy.

Although the amplitude of the ^1H signals was reduced with the ^{31}P BC inserted, we were able to optimize the B_1^+ field and use this to enhance signals. Moreover, the irradiation of the water spins with low RF power led to a time-averaged maximum input power of 10.9 W. Assuming the weight of an average head to be approximately 5 kg, this leads to a worst-case head-averaged

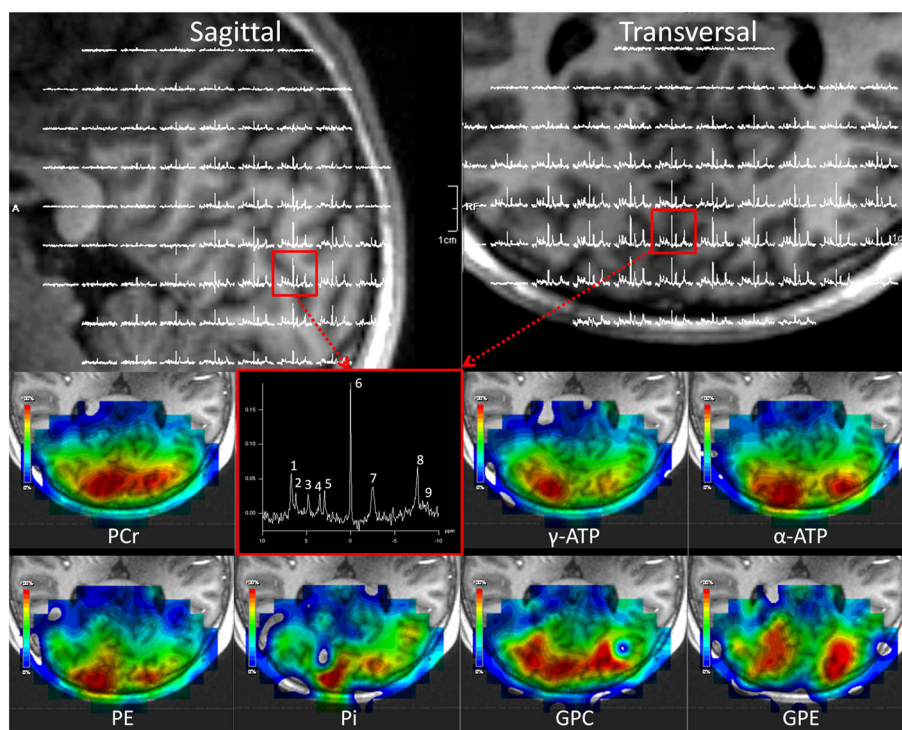


Figure 7. High-resolution 3D MRSI using all available options to increase SNR. The signals were enhanced using NOE and were received with the local receive array. Note the exquisite quality of the spectra. Top left, a sagittal view of the human brain overlapped with ^{31}P spectra as acquired with the receive array. Top right, a transversal view of the human brain also overlapped with a spectral map covering the occipital lobe. Bottom two rows, metabolite maps of seven different ^{31}P compounds. The colors show the distribution of the metabolites (scaled 0–100%) represented by the fitted integral. Note that in only two voxels were low-SNR metabolites (P_i and GPC) fitted incorrectly within the FOV of the array coil. Moreover, note the difference in spatial distributions of the different metabolites, which arise not only from the B_1 -receiving profile (anterior–posterior), but also from differences between gray and white matter (left–right). A spectrum with high quality (3 cm^3 voxel), as acquired in 15 min in the occipital lobe (red box), is shown too. Not shown in this spectrum is the β -ATP, as the bandwidth of the pulse to properly excite this metabolite was insufficient. (1) PE, (2) PC, (3) P_i , (4) GPE, (5) GPC, (6) PCr, (7) γ -ATP, (8) α -ATP and (9) NADH.

SAR of 2.18 W/kg , which is already well below the IEC-defined limit of 3.2 W/kg for the head. Within this approximation losses inside the coil (e.g. feed network, coil elements, etc.) are also present, thus the head-averaged SAR would be reduced even further. Furthermore, when using phased array coils for exciting the MR signal instead of volume resonators, SAR deposition can be reduced significantly (up to 50%) while optimizing the B_1^+ distribution, as has been shown by van den Bergen *et al.* in the pelvic area (32). Although this was investigated at 3 and 7 T with a TEM coil, it was shown by Wang *et al.* that SAR levels are lower in microstrip coil designs at 7 T (33). These findings support the usage of this 8-CH multiple-array antenna. Moreover, the meander structures in the element decrease intrinsic coupling of the elements, and reduce the magnitude of the electric field at the ends of the elements (20). A striking fact from the same study is that SAR levels for BC coils, such as our new design for ^{31}P , were higher at 7 T. Note that we optimized this BC coil for a lower frequency (120.3 MHz), and when using volume coils at these frequencies the head-averaged SAR is usually the most critical aspect.

Most studies on ^{31}P in the human brain at 7 T have been using surface coils to excite and receive the MR signal (14,34,35), except for that by Zhu *et al.* (36), who used a CP dual-frequency volume RF coil. Although surface coils have a higher SNR, their B_1 fields are inhomogeneous, hence the flip angle becomes position dependent should one use a hard pulse for excitation. By using adiabatic pulses these limitations can be circumvented,

but at a cost of markedly increased pulse duration and concomitant increase in SAR deposition. Using the homogenous volume resonator present here allowed us to avoid SAR demanding adiabatic pulses, but rather use short (0.3 ms) hard pulses that have sufficient bandwidth to excite the spectrum (except β -ATP). Note that Zhu *et al.* were not able to use these in their study (36).

In conclusion, the developed coil setup can be used to excite ^1H and ^{31}P signals at an ultra-high field strength of 7 T. ^{31}P signals can be acquired with an increased SNR by exploiting NOE enhancement and by receiving the signals with a local receive array.

Acknowledgements

We thank M.J. van Uden and A. Veltien for the extensive discussions about safety, design, construction, and implementation of coilfiles, E.W.J. Philips for implementing the WSVD code into the pulse sequence, Y. Noureddine for his help setting up the field probe measurements, and Elisabeth Weiland from Siemens Healthcare for providing Metabolite Report. Part of this work was supported by Grant 243115 from the European Research Council under the European Community's Seventh Framework Programme (FP7/2007–2013). C.T. Rodgers is funded by the Wellcome Trust and the Royal Society (Grant Number 098436/Z/12/Z).

REFERENCES

- Hugg JW, Matson GB, Twieg DB, Maudsley AA, Sappey-Marini D, Weiner MW. Phosphorus-31 MR spectroscopic imaging (MRSI) of normal and pathological human brains. *Magn. Reson. Imaging* 1992; 10(2): 227–243.
- Rodgers CT, Clarke WT, Snyder C, Vaughan JT, Neubauer S, Robson MD. Human cardiac ^{31}P magnetic resonance spectroscopy at 7 Tesla. *Magn. Reson. Med.* 2014; 72(2): 304–315.
- Wright SM, Wald LL. Theory and application of array coils in MR spectroscopy. *NMR Biomed.* 1997; 10(8): 394–410.
- Tannus A, Garwood M. Adiabatic pulses. *NMR Biomed.* 1997; 10(8): 423–434.
- Avdievich NI, Hetherington HP. 4 T actively detuneable double-tuned $^1\text{H}/^{31}\text{P}$ head volume coil and four-channel ^{31}P phased array for human brain spectroscopy. *J. Magn. Reson.* 2007; 186(2): 341–346.
- Roemer PB, Edelstein WA, Hayes CE, Souza SP, Mueller OM. The NMR phased array. *Magn. Reson. Med.* 1990; 16(2): 192–225.
- Keil B, Wald LL. Massively parallel MRI detector arrays. *J. Magn. Reson.* 2013; 229: 75–89.
- Rodgers CT, Robson MD. Receive array magnetic resonance spectroscopy: whitened singular value decomposition (WSVD) gives optimal Bayesian solution. *Magn. Reson. Med.* 2010; 63(4): 881–891.
- Rodgers CT, Robson MD. Coil combination for receive array spectroscopy: are data-driven methods superior to methods using computed field maps? *Magn. Reson. Med.* 2015. DOI:10.1002/mrm.25618.
- Vaughan JT, Snyder CJ, DelaBarre LJ, Bolan PJ, Tian J, Bolinger L, Adriani G, Andersen P, Strupp J, Ugurbil K. Whole-body imaging at 7 T: preliminary results. *Magn. Reson. Med.* 2009; 61(1): 244–248.
- Metzger GJ, Snyder C, Akgun C, Vaughan T, Ugurbil K, Van de Moortele PF. Local B_1^+ shimming for prostate imaging with transmit arrays at 7 T based on subject-dependent transmit phase measurements. *Magn. Reson. Med.* 2008; 59(2): 396–409.
- Luyten PR, Bruntink G, Sloff FM, Vermeulen JW, van der Heijden JJ, den Hollander JA, Heerschap A. Broadband proton decoupling in human ^{31}P NMR spectroscopy. *NMR Biomed.* 1989; 1(4): 177–183.
- Lagemaat MW, Maas MC, Vos EK, Bitz AK, Orzada S, Weiland E, van Uden MJ, Kobus T, Heerschap A, Scheenen TW. ^{31}P MR spectroscopic imaging of the human prostate at 7 T: T_1 relaxation times, Nuclear Overhauser Effect, and spectral characterization. *Magn. Reson. Med.* 2014; 73(3): 909–920. DOI:10.1002/mrm.25209.
- Lei H, Zhu XH, Zhang XL, Ugurbil K, Chen W. In vivo ^{31}P magnetic resonance spectroscopy of human brain at 7 T: an initial experience. *Magn. Reson. Med.* 2003; 49(2): 199–205.
- Klomp DW, Wijnen JP, Scheenen TW, Heerschap A. Efficient ^1H to ^{31}P polarization transfer on a clinical 3 T MR system. *Magn. Reson. Med.* 2008; 60(6): 1298–1305.
- Wijnen JP, Scheenen TW, Klomp DW, Heerschap A. ^{31}P magnetic resonance spectroscopic imaging with polarisation transfer of phosphomono- and diesters at 3 T in the human brain: relation with age and spatial differences. *NMR Biomed.* 2010; 23(8): 968–976.
- van der Kemp WJ, Boer VO, Luijten PR, Klomp DW. Increased sensitivity of ^{31}P MRSI using direct detection integrated with multi-echo polarization transfer (DIMEPT). *NMR Biomed.* 2014; 27(10): 1248–1255.
- van der Kemp WJ, Boer VO, Luijten PR, Wijnen JP, Klomp DW. Increase in SNR for ^{31}P MR spectroscopy by combining polarization transfer with a direct detection sequence. *Magn. Reson. Med.* 2012; 68(2): 353–357.
- Orzada S, Kraff O, Brote I, Schäfer LC, Bahr A, Bolz T, Maderwald S, Ladd ME, Bitz AK. 8-channel transmit/receive head coil for 7 T human imaging using intrinsically decoupled strip-line elements with meanders. *Proc. Int. Soc. Magn. Reson. Med.* 2009; 17: 3010.
- Rietsch SHG, Quick HH, Orzada S. Impact of different meander sizes on the RF transmit performance and coupling of microstrip line elements at 7 T. *Med. Phys.* 2015; 42(8): 4542–4552.
- Leifer MC. Resonant modes of the birdcage coil. *J. Magn. Reson.* 1997; 124(1): 51–60.
- Chin CL, Collins CM, Li SH, Dardzinski BJ, Smith MB. BirdcageBuilder: design of specified-geometry birdcage coils with desired current pattern and resonant frequency. *Concepts Magn. Reson.* 2002; 15(2): 156–163.
- Meyerspeer M, Roig ES, Gruetter R, Magill AW. An improved trap design for decoupling multinuclear RF coils. *Magn. Reson. Med.* 2013; 72(2): 584–590. DOI:10.1002/mrm.24931.
- Hoult DI, Lauterbur PC. The sensitivity of the zeugmatographic experiment involving human samples. *J. Magn. Reson.* 1979; 34(2): 425–433.
- Bitz A, Kraff O, Orzada S, Maderwald S, Brote I, Johst S, Ladd M. Assessment of RF safety of transmit coils at 7 Tesla by experimental and numerical procedures. *Proc. Int. Soc. Magn. Reson. Med.* 2011; 19: 490.
- Shaka AJ, Keeler J, Freeman R. Evaluation of a new broadband decoupling sequence: WALTZ-16. *J. Magn. Reson.* 1983; 53(2): 313–340.
- Bitz A, Brote I, Orzada S, Kraff O, Maderwald S, Quick H, Yazdandbakhsh P, Solbach K, Bahr A, Bolz T, Wickdow K, Schmitt F, Ladd M. An 8-channel add-on RF shimming system for whole-body 7 Tesla MRI including real-time SAR monitoring. *Proc. Int. Soc. Magn. Reson. Med.* 2009; 17: 4767.
- van de Bank BL, Voogt IJ, Italiaander M, Stehouwer BL, Boer VO, Luijten PR, Klomp DW. Ultra high spatial and temporal resolution breast imaging at 7 T. *NMR Biomed.* 2012; 26(4): 367–375. DOI:10.1002/nbm.2868.
- Edelstein WA, Hardy CJ, Mueller OM. Electronic decoupling of surface-coil receivers for NMR imaging and spectroscopy. *J. Magn. Reson.* 1986; 67(1): 156–161.
- Hardy CJ, Bottomley PA, Rohling KW, Roemer PB. An NMR phased array for human cardiac ^{31}P spectroscopy. *Magn. Reson. Med.* 1992; 28(1): 54–64.
- Lee RF, Giaquinto R, Constantinides C, Souza S, Weiss RG, Bottomley PA. A broadband phased-array system for direct phosphorus and sodium metabolic MRI on a clinical scanner. *Magn. Reson. Med.* 2000; 43(2): 269–277.
- van den Bergen B, Van den Berg CA, Bartels LW, Lagendijk JJ. 7 T body MRI: B_1 shimming with simultaneous SAR reduction. *Phys. Med. Biol.* 2007; 52(17): 5429–5441.
- Wang CS, Shen GX. B_1 field, SAR, and SNR comparisons for birdcage, TEM, and microstrip coils at 7 T. *J. Magn. Reson. Imaging* 2006; 24(2): 439–443.
- Chmelík M, Just Kukurová I, Gruber S, Krššák M, Valkovič L, Trattnig S, Bogner W. Fully adiabatic ^{31}P 2D-CSI with reduced chemical shift displacement error at 7 T — GOIA-1D-ISIS/2D-CSI. *Magn. Reson. Med.* 2013; 69(5): 1233–1244.
- Lu M, Chen W, Zhu X-H. Field dependence study of *in vivo* brain ^{31}P MRS up to 16.4 T. *NMR Biomed.* 2014; 27(9): 1135–1141.
- Zhu XH, Qiao H, Du F, Xiong Q, Liu X, Zhang X, Ugurbil K, Chen W. Quantitative imaging of energy expenditure in human brain. *Neuroimage* 2012; 60(4): 2107–2117.